# 8 March 2010 Elazığ-Kovancılar (Turkey) Earthquake: Observations on Ground Motions and Building Damage

Sinan Akkar[1], Alper Aldemir[1], Aysegul Askan[1], Sadık Bakır[1], Erdem Canbay[1], Ozan Demirel[1], Altug Erberik[1], Zeynep Gülerce[1], Polat Gülkan[1], Erol Kalkan[2], Surya Prakash[3], Abdullah Sandıkkaya[1], Volkan Sevilgen[2], Beliz Ugurhan[1], Emrah Yenier[1]

1 Earthquake Engineering Research Center, Middle East Technical University, 06531 Ankara, Turkey

2 US Geological Survey, Menlo Park, CA 94025

3 National Institute of Disaster Management, New Delhi 110-002, India

## Introduction

An earthquake of $M_L$=5.8 occurred in the Elazığ region of Eastern Turkey on March 08, 2010 at 02:32:34 UTC. Earthquake Research Department (ERD) of Disaster and Emergency Management Authority of Turkey (DEMA) reported the epicenter of the earthquake as 38.7752N - 40.0295E with a focal depth of 5 km. 42 people lost their lives and 137 were injured during the event. The earthquake was reported to be on the left-lateral strike-slip East Anatolian Fault (EAF) which is one of the two major active fault systems in Turkey. Teams from the Earthquake Engineering Research Center of the Middle East Technical University (EERC-METU) visited the earthquake area in the aftermath of the mainshock. Their reconnaissance observations were combined with interpretations of recorded ground motions for completeness. This article summarizes observations on building and ground damage in the area, providing a discussion of the recorded motions. No significant observations in terms of geotechnical engineering were made.

The affected area is a sparsely populated rural region in Turkey, so the earthquake remained in the headlines of the national media only briefly. We provide an account of this earthquake because it is our policy to record the effects of every earthquake for later reference.

**Seismotectonics of the Region**

The major tectonic structure in Turkey is the North Anatolian Fault Zone (NAFZ) with right-lateral faulting extending from Istanbul in the West to Karlıova in the East. This fault zone has produced several large earthquakes (Ms>7) with surface rupturing during the twentieth century with a westward migrating sequence demonstrated in Figure 1 (Barka, 1996; Utkucu et al., 2003). Around Karlıova region, NAFZ joins the southwest-trending East Anatolian Fault Zone (EAFZ). The EAFZ is predominantly left-lateral strike-slip in nature; but its faulting is less continuous, less localized than that of NAFZ (Ambraseys, 2009). EAFZ has nucleated relatively small magnitude earthquakes in the twentieth century (Figure 1).

Recent GPS data indicates that the slip rate in EAFZ has an upper bound of 81 mm/year (Ambraseys, 2009). The epicenter (by DEMA) of 8 March 2010 Elazığ-Kovancılar earthquake is in the segmented fault region of the EAFZ to the south of Karakoçan region with a left-lateral strike-slip faulting mechanism. However, no surface rupturing was observed in the field. Figure 1 shows the strong motion stations that recorded the mainshock and the active faults in the region.

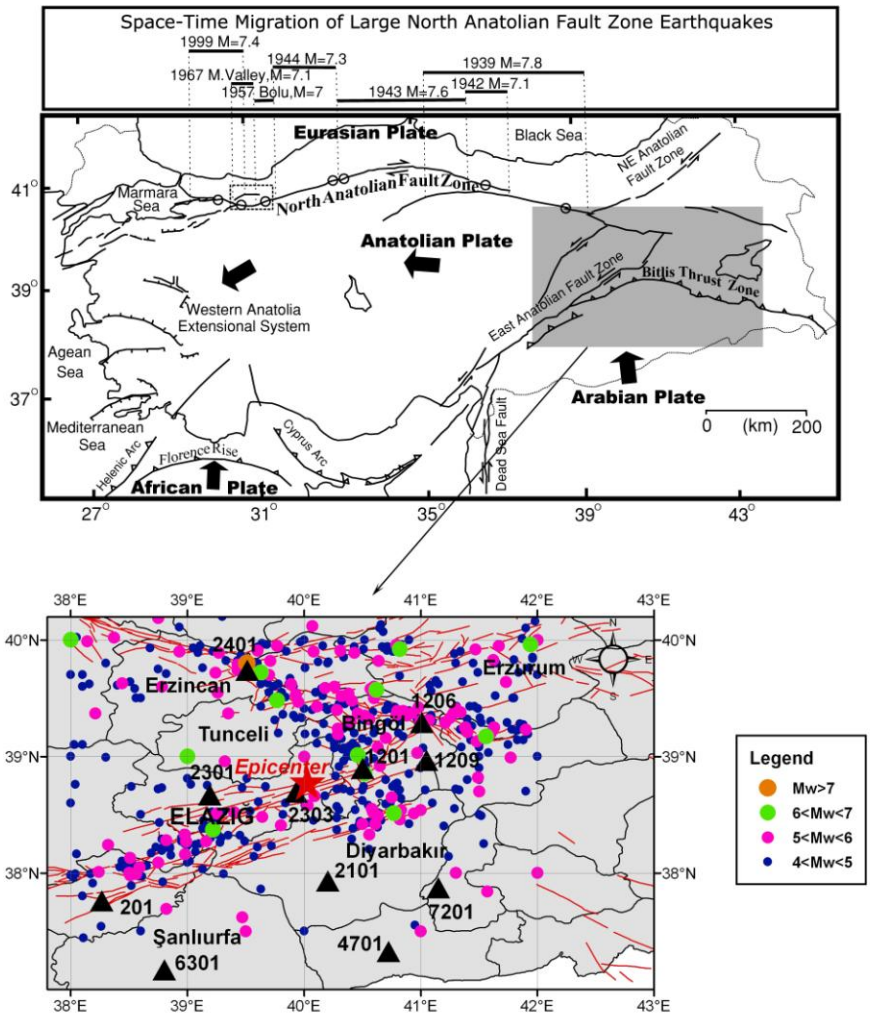


**Figure 1**. Tectonic structure of Turkey (top) and seismicity of the EAFZ during the last century (bottom) (Top figure is adapted from Barka (1996) and Utkucu et al. (2003)). The red star indicates the epicenter of the Elazığ-Kovancılar earthquake whereas strong motion stations operated by DEMA are shown with black triangles. Active faults in the region, which are shown in red, are adapted from the active fault map of Saroglu et al. (2002).

**Postulated Stress Transfer**

A static Coulomb stress transfer model has been calculated for the Kovancılar earthquake to promote failure by 0.1 bar on the East Anatolian Fault as shown in Figure 2. There is evidence of 0.1 bar of stress increase triggering seismicity on the adjacent active faults (Lin and Stein, 2004; Toda *et al*., 2005). Rupture orientation of the 2010 Elazığ-Kovancılar earthquake is inferred from the aftershock distribution and the USGS body wave focal mechanism which is left lateral strike slip fault with 47º strike, 75º dip and -4º rake. In the Coulomb calculation, a 10 by 7 km rupture area with a 0.5 m uniform slip is assumed as the Coulomb source fault based on Wells and Coppersmith (1994) relationship.

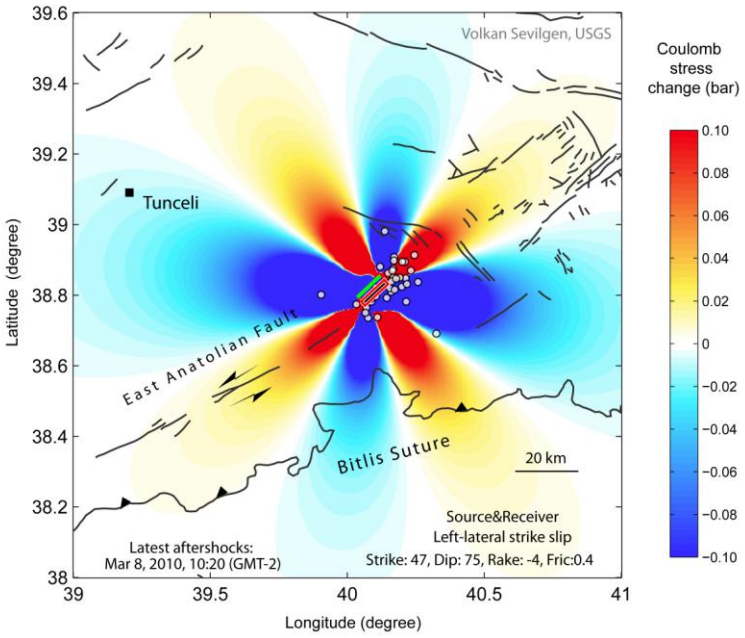


**Figure 2.** Elazığ-Kovancılar earthquake increased the static Coulomb stress on the East Anatolian Fault. Green line is the surface trace of the Coulomb source, red rectangle is the Coulomb source fault. Black circles are the aftershocks.

**Recorded Ground Motions and Ground Motion Predictions**

Ground motions recorded at the stations shown in Figure 1 are demonstrated in terms of three-component acceleration time histories on Figure 3. Peak ground accelerations and spectral accelerations computed at T = 0.2 s and 1.0 s are then compared with predictions. Several "ground motion prediction equations" (GMPEs) are used to characterize ground motion variation with distance. Recorded raw acceleration time series were first corrected by trend removal including pre-event mean, and then uniformly filtered by $5^{th}$-pole Butterworth filter with cut-off frequencies of 0.2 Hz and 20 Hz, respectively. Baseline correction based on segmental polynomial was applied to assure that displacement and velocity converge to zero at the termination of each record. Using the corrected records, five percent damped response spectral ordinates for each component of ground motion were computed. Peak-ground acceleration (PGA) and spectral accelerations (SA) at 0.2 s and 1.0 s for eleven records are tabulated in Table 1. Also listed are the characteristics of stations and distance metrics. The closest station was at 17 km to the epicenter, while the remaining ones were at moderate to long distances away. Selected GMPEs utilize two unique definitions of distance parameter specific to the model. In the first case, the distance measure is the Joyner-Boore distance definition ($R_{jb}$), defined as the closest distance from the recording station to the surface projection of the fault rupture plane (Boore et al., 1997). In the second case, the distance measure is the "closest fault distance" ($R_{CL}$) defined as the closest distance to co-seismic rupture plane (Campbell and Bozorgnia, 2008). GMPEs selected are those of Kalkan and Gülkan (2004) [KG04], Boore and Atkinson (2008) [BA07], and Akkar and Cagnan (2010) [AC10] utilizing $R_{jb}$ definition, and Grazier and Kalkan (2007) [GK07], Campbell and Bozorgnia (2008) [CB08], and Chiou and Youngs (2008) that use "closest fault distance". Among them, the KG04 and AC10 are based on indigenous datasets compiled from Turkish earthquakes. The BA08, CB08, CY08 and GK07 are based on the NGA[1] database, which also contains earthquake records from Turkey.

[1] NGA stands for Next Generation Attenuation project (Power et. al., 2006)

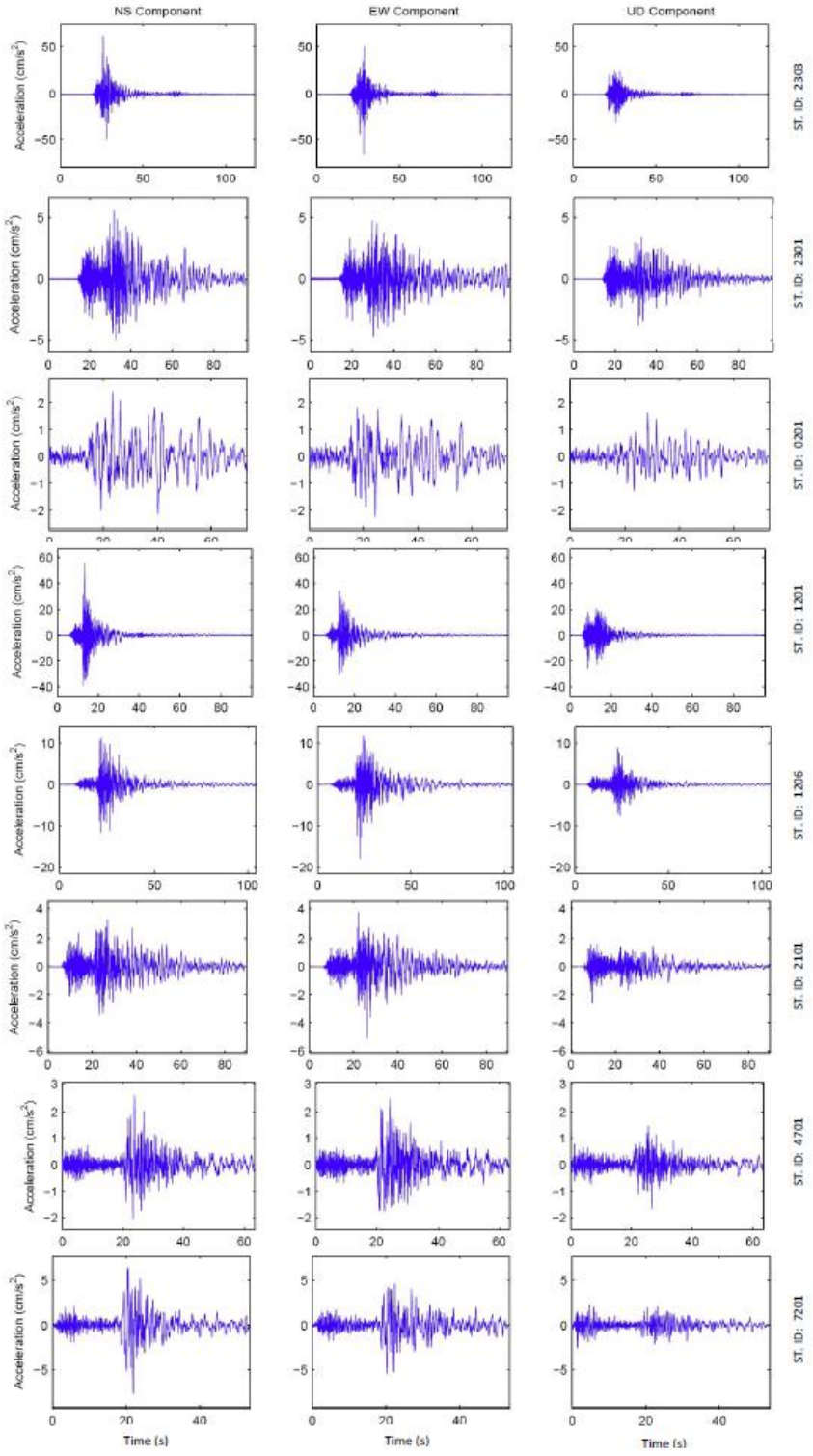


**Figure 3.** Acceleration time series of the processed ground motions recorded from the 08/03/2010 02:32:29 Elazığ-Kovancılar, Earthquake. North-South (NS), East-West (EW), and Up-Down (UD) components are plotted left, middle and right columns, respectively.

Figure 4.a compares the PGA, SA at 0.2 s and 1.0 s with six GMPEs based on the two different distance measures. The attenuation curves are plotted for the average $V_{S30}$ of eleven stations ($V_{S30,ave}$ = 449 m/s), which corresponds to NEHRP site class $S_C$. Maximum values from two horizontal components of each record are utilized (shown by filled circles). Because the AC10, BA08, CB08 and CY08 predict geometric mean of ground motion, their predictions are adjusted for maximum horizontal component by multiplying their predictions with 1.11, 1.11 and 1.18 for PGA, SA at 0.2 s and 1.0 s, respectively. These adjustment factors were adapted from the Campbell and Bozorgnia (2008). The other GMPEs (KG04 and GK07) predict the maximum of the two horizontal components.

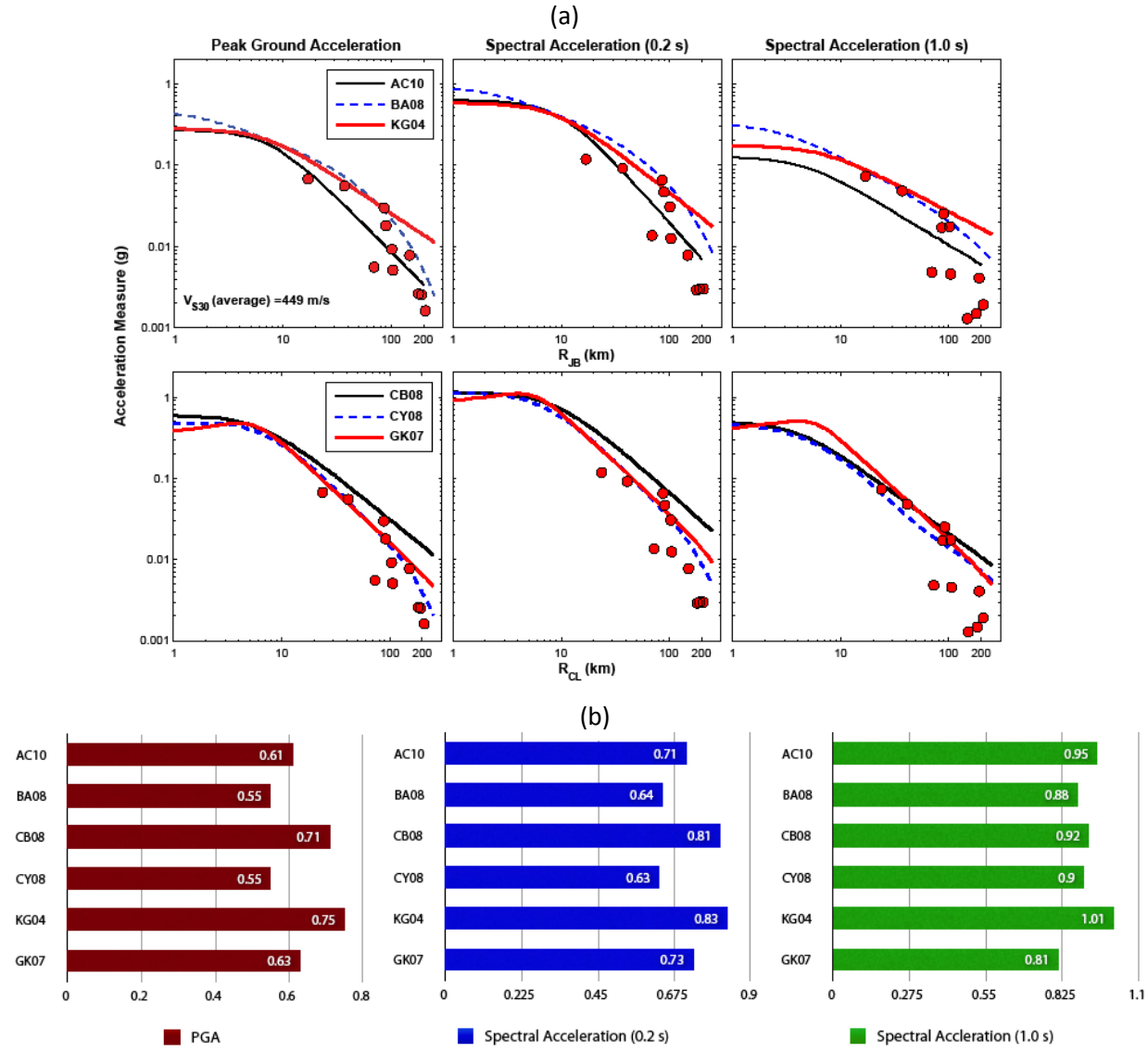


**Figure 4. a)** Comparison of PGA, SA at T = 0.2 s and 1.0 s values recorded from the main shock (M6.0 on strike-slip fault at 5 km depth) with six different GMPEs considering two distance measures. [Top panels] Predictions considering $R_{JB}$ for AC10 – Akkar and Cagnan, 2010; BA08 – Boore and Atkinson, 2008; KG04 – Kalkan and Gülkan, 2004; [Bottom panels] Predictions considering $R_{CL}$ for CB08 – Campbell and Bozorgnia, 2008; Chiou and Youngs, 2008; GK07 – Graizer and Kalkan, 2007. Ground motion data shows faster attenuation at far distances due to apparent regional low Q (Zor et al., 2007). **b)** Standard error ($\sigma_{\ln Y}$) of predictions computed for each GMPE for PGA, SA (0.2 s) and SA (1.0 s) using maximum horizontal components from eleven ground motion records. The average standard error of six GMPEs is 0.63, 0.73 and 0.91 respectively for PGA, SA at 0.2 s and 1.0 s.

As seen in Figure 4.a, the GMPEs indicate an overall good fit to recorded data up to about 100 km from the fault for PGA, SA at 0.2 s and 1.0 s. Beyond 100 km, there is notable overestimation. Actual data show faster attenuation in the order of $R^{-4}$ beyond 100 km, and slower attenuation in the order of $R^{-1.5}$ at closer distances to fault. Faster attenuation of ground motion is due to the low Q of the crustal structure in this particular region of Eastern Turkey (Zor et al., 2007). For PGA, faster attenuation of PGA ($R$ > 100 km) is reasonably captured by AC10, BA08, CY08 and GK07; the CB08 and KG04 over-predict the actual data beyond 100 km. For SA at 0.2 s at $R$ > 100 km, the AC10, CY08 and GK07 are the only three models providing the best predictions. For SA at 1.0s, predictions of BA08, CB08, CY08 and GK07 within 20 to 100 km are similar to each other, and fit reasonably well to actual data. Particularly for SA at 1.0 s, predictions of AC10 at all distances are much lower than those of other five models. For half of the data points, all GMPEs over predict the SA at 1.0 s, particularly data beyond 100 km, the over prediction is more significant for KG04. To quantify the quality of fit, the standard error ($\sigma_{lnY}$) of prediction for each GMPE are computed based on residuals corresponding to eleven data points. The comparisons of standard error are demonstrated in Figure4.b for PGA, SA at 0.2 s and 1.0 s.

**Effects of the Earthquake on Buildings**

The earthquake has caused major structural damage in few villages (Okçular, Göçmezler, Yukarı Kanatlı, Yukarı Demirci and Tabanözü shown in Figure 5) where all the fatalities were reported after the earthquake. Nearby towns and provinces were not seriously affected from the earthquake. The main reason of widespread damage in villages close to the epicenter can be explained by considering the building typology and the construction practice in the affected region.


**Figure 5.** The villages which had severe structural damage during the 8 March 2010 Kovancılar earthquake

**Local Construction Materials**

Dictated by the climate of the region, standard of living and buildings practices of the region, adobe, stone and hollow factory brick are the most commonly used construction materials. Adobe is produced from local clayey soil mixed with straw and dried under the sun. Although there are no material tests available, from field observations (adobe is easily broken into small pieces by hand) it might be inferred that adobe units have very low strength with respect to the density of the material. Local stone is used in an irregular fashion without shaping into regular geometry. Hollow factory brick is used as a load bearing material although this is not allowed by the Turkish Earthquake Code (2007). Mud is utilized both as bonding material between brick units and for plastering.

Rural masonry buildings are characterized in two different ways according to the roof material used. First one is heavy condensed soil which is laid over the slab supported by wooden logs. Second one is light metal sheets which are supported by wooden girders and columns (Figure 6).

**Figure 6. a)** Heavy earthen roofs **b)** Light sheet metal roof supported by wooden logs

Significant percentage of the building stock in the affected area is composed of one or two story masonry buildings constructed with thick adobe or stone walls, very low quality mortar and wooden beams covered by either earthen or sheet metal roofs. It might be appropriate to classify buildings in the affected area into four groups depending on their structural characteristics (Table 2). In order to eliminate the country specific characteristics of building typology in the affected region, a vulnerability class is assigned to each building type according to European Macroseismic Scale (Grünthal 1998). EMS vulnerability classes range between A and F, for which letter A represents the most vulnerable class.

Type-I buildings constitute the most vulnerable structural system among others. Many such buildings have collapsed in past earthquakes resulting in loss of lives. Thickness of the condensed soil at the roof is in between 30-50 cm. Such heavy roofs induce large inertial forces during earthquake which result in high stresses on low strength walls. Roof cave-in becomes a death trap for the people inside the building (Figure 7.a). EMS vulnerability class A can be assigned to these type of buildings.

Type-II buildings are more resistant to earthquake effects than Type-I buildings due to their lighter roofs, properly placed horizontal bond beams, relatively better corner connections and better vertical alignment of openings. This type of buildings is not earthquake resistant but can withstand earthquakes of moderate intensity since some basic rules of thumb have been considered during the construction of these buildings. Therefore, the buildings in this category were observed to experience

some damage during the Elazığ Kovancılar earthquake but total collapse was usually prevented (Figure 7.b). EMS vulnerability class B is assigned to these type of buildings.

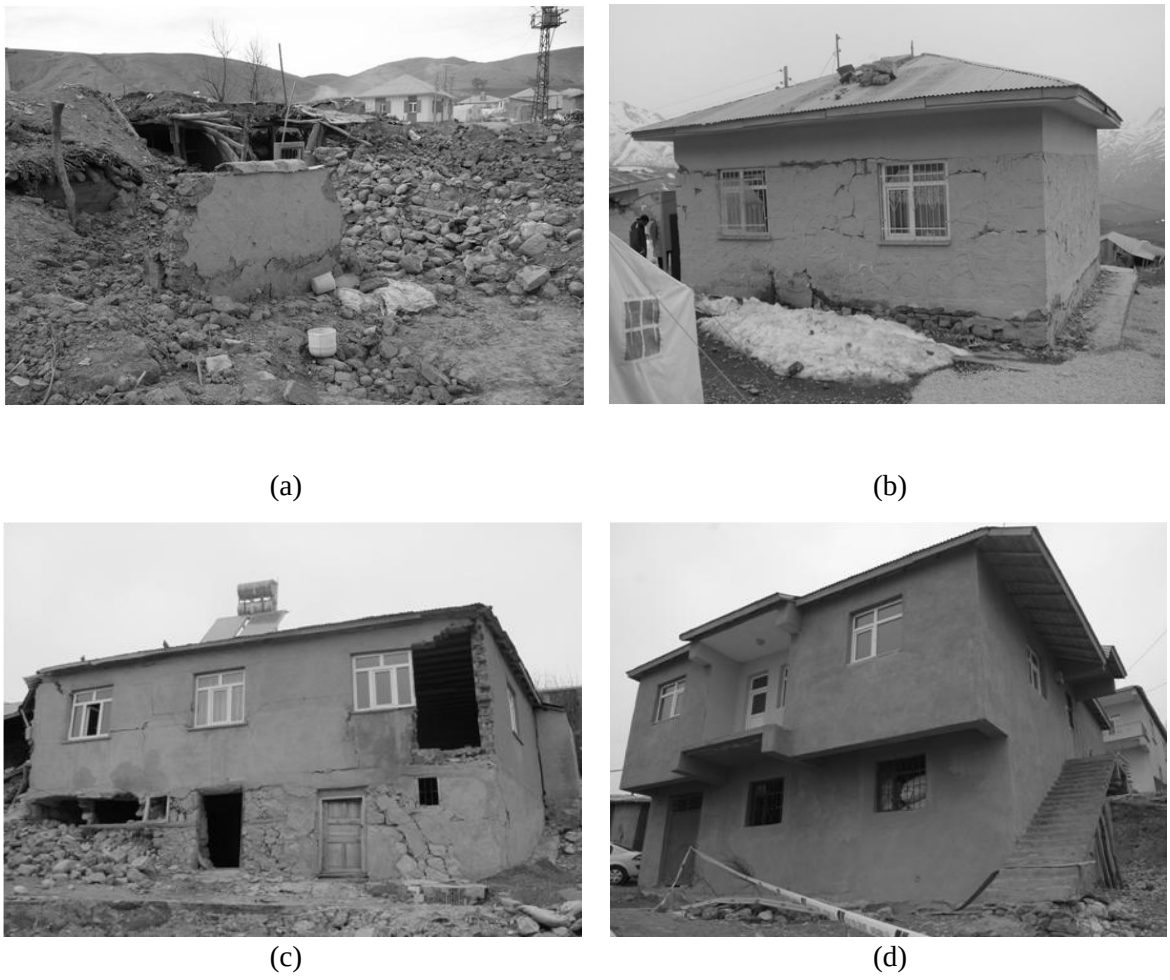

(a) (b)

(c) (d)

**Figure 7.** Local buildings classified according to structural typology. Examples of **a)** Type-I, **b)** Type-II, **c)** Type-III and **d)** Type-IV buildings

Type-III buildings are the most complex structural systems which are frequently encountered in the field. Their ground story is often used as barn or for storage. It is generally made of stone, but there are also cases where adobe is used. Second story is used for residential purposes and is generally made of hollow factory brick. The main problem in this type of buildings is the incompatibility of the materials used for different stories and their improper connection to each other. Partial out of plane

collapse of second storey walls is a typical damage pattern for this type of buildings (Figure 7.c). EMS vulnerability class A can be assigned to these type of buildings.

Type-IV buildings are rarely observed in the field. Reinforced concrete columns, beams and slabs are the load bearing members. Unlike Type-I, -II and -III, rigid diaphragm action is valid for this type of buildings due to stiff concrete slab. However, the material quality is poor and the construction practice does not generally conform to fundamental requirements of earthquake resistant design. It should not be surprising that this type of buildings exhibited an adequate performance with limited damage during such a moderate earthquake (Figure 7.d). EMS vulnerability class C can be assigned to these type of buildings.

**Observed Structural Damage**

***Rural Masonry Buildings (Type-I, Type-II and Type-III)***

The failure modes of rural masonry buildings observed in the field are out-of-plane failure of walls and gable end walls, in-plane failure of walls, total or partial collapse of the buildings due to the absence of structural integrity and collapse of the roof. Out-of-plane failure of walls and gable end walls can easily be inferred from the site observations that this type of failure mode is frequently encountered. The main causes of this failure mode are stability problems that arise from large unsupported wall lengths in the absence of lateral supporting walls, (Figure 8.a), poor wall-to-floor connections (Figure 8.b) and poor wall-to-wall connections (Figure 8.c). In the absence of connecting units and proper detailing at the connections of perpendicular walls, the walls are separated from each other, behaving like single walls that are weak in the out-of-plane direction. Collapse of gable end wall was also encountered during field investigations (Figure 8.d).

For Types-I and –III buildings, in-plane failure modes were not frequently observed since the buildings are so poorly constructed and detailed that the walls generally collapsed in the out-of-plane direction. For Type-II buildings, in the cases where out-of-plane failure was prevented, in-plane damage was

observed in the form of horizontal cracks indicating sliding and rocking behavior and X-shaped cracks indicating diagonal shear mechanism.

Many buildings of Type-I collapsed due to the absence of structural integrity of vertical load carrying members. Because wall-to-wall and wall-to-floor connections are not adequate. The early indications of this failure mode appear as damage at corners of walls and at top of the walls where they are supposed to be connected to the floor slab.

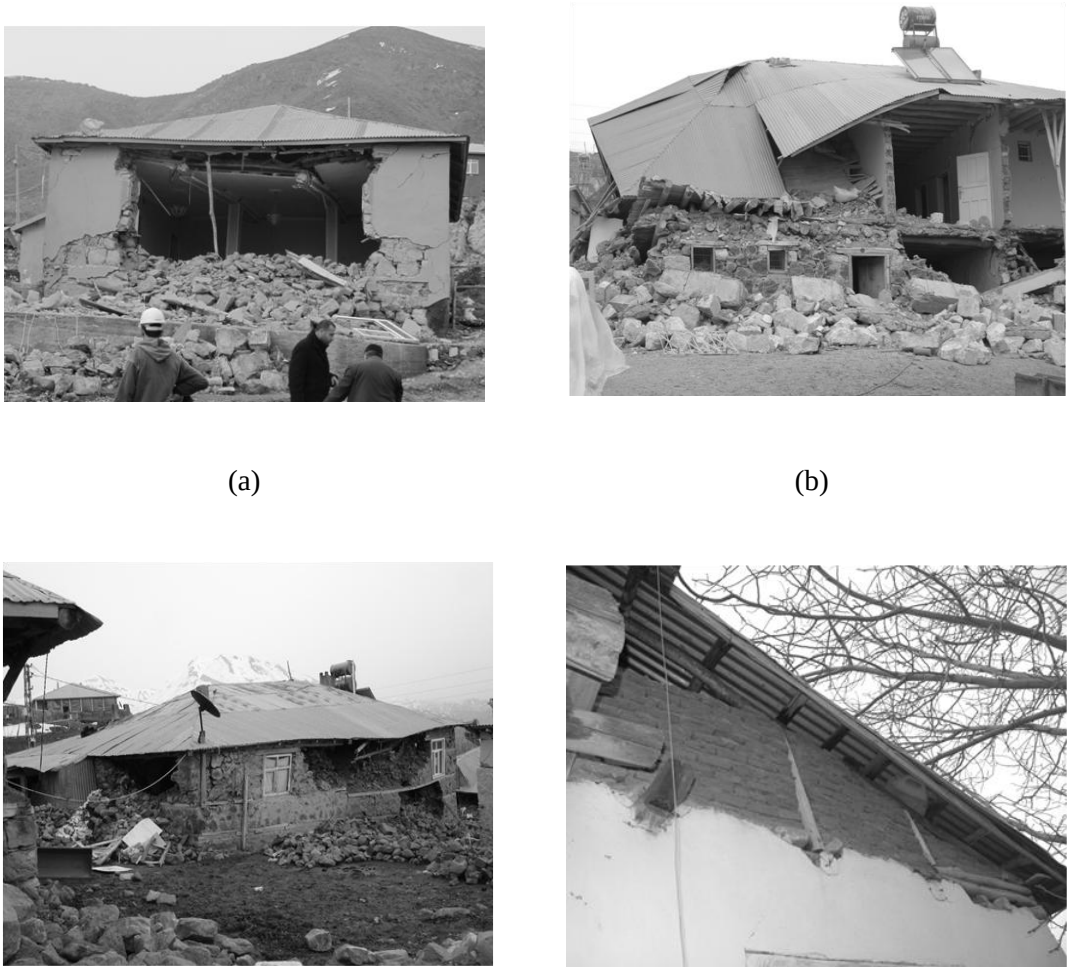

(a) (b)

(c) (d)

**Figure 8.** Out of plane failures of walls due to **a)** large unsupported wall length, **b)** poor wall-to-wall connection, **c)** poor wall-to-floor connection, **d)** unstable gable end wall

***Reinforced Concrete Frame Buildings (Type-IV)***

With a few exceptions, the reinforced concrete buildings performed well during the earthquake. Most of them show light or no damage with hairy cracks or non-structural damages. Consequently, they could be occupied immediately after the earthquake.

***School Buildings***

Primary school buildings in the affected villages were stone masonry buildings of Type-I and –II and they experienced significant damage during the earthquake. The school building in Yukarı Demirci collapsed during the earthquake. A closer look at the collapsed school building revealed that there was a ring beam at the roof level of the building which was supposed to be made of reinforced concrete, but it was "reinforced stone", i.e. pieces of crushed stone was filled inside the reinforcement cage with inadequate amount of mortar to hold the pieces together and to fill the spaces (Figure 9). Primary school buildings in other two villages were also severely damaged. Hence, it was fortunate that the earthquake did not happen during day-time when the students were studying in their classes.

(a) (b)

**Figure 9.** Collapsed stone masonry school building in Yukarı Demirci village **a)** exterior view, **b)** Closer look at the reinforced stone ring beam at the roof level

***Mosques and minarets***

Mosques and minarets were also damaged in the villages during the earthquake. Figure 10.a shows the interior view of the mosque in Yukarı Kanatlı village. It was a stone masonry building of Type-B with out-of-plane damage to its exterior walls. Minarets in three of the villages were also destroyed (Figure 10.b).

(a) (b)

**Figure 10. a)** Interior view of the damaged mosque in Yukarı Kanatlı village, **b)** damaged minaret in Yukarı Demirci village.

**Quantification of Observed Damage**

Based on the field observations, it is possible to quantify the observed damage in terms of damage levels of building classes in the vicinity of mostly affected villages. For quantification of damage, European Macroseismic Scale (EMS) was employed (Grünthal 1998). EMS scale provides damage grade charts separately for masonry and reinforced concrete structures. Damage grades range between 1 and 5, the former representing negligible to slight damage and the latter representing total collapse or destruction.

According to the field observations, most of the buildings in Type I (Class A according to EMS) collapsed (Grade 5 according to EMS), most of the buildings in Type II (Class B according to EMS) suffered moderate damage (Grade 3 according to EMS), most of the buildings in Type III (Class A

according to EMS) were heavily damaged (Grade 4 according to EMS) and most of the buildings in Type-IV (Class C according to EMS) were slightly damaged (Grade 2 according to EMS). Comparing the observed damage with the definitions given in EMS Intensity Scale, it is observed that EMS Intensity VIII (heavily damaging) can be assigned to the most heavily affected region (including villages Okçular, Yukarı Kanatlı, Tabanözü and Yukarı Demirci) for March 2010 earthquake.

A final comment on building practices is illustrated vividly in Figure 11 that shows damage to the type of rural buildings that have been described in this report. With little differences in the way dwellings are built (usually by their owners) between 1977 and 2010, there is also little difference in their seismic capacities. Minor improvement in details would have served to avoid collapses and the resulting losses of life.

(a) (b)

**Figure 11.** Photos taken from collapsed rural masonry buildings **a)** during the Elazığ Palu earthquake in 1977 **b)** Elazığ Kovancılar earthquake in 2010

**Closing Observations**

The Elazig-Kovancılar earthquake of March 8, 2010 was not a major seismic event, but it confirmed the scientific benefit of Turkey's expanded national strong motion network because it provided data for

a small-magnitude event at moderate and long distances. The regional variation of recorded ground motions shows major differences from global equations of both domestic and global character.

The engineering reconnaissance showed that despite important advances toward achievement of seismic safety elsewhere in the country, rural areas with low economic status still lack adequate life safety. Of particular concern is the poor performance of school buildings, the most widely used facilities. An inspection program for school buildings similar to those that were damaged beyond repair must be immediately undertaken.

**Acknowledgments**

The two EERC-METU teams that visited the stricken area within ten days of the event were the recipients of the hospitality and material support of Fırat University. We thank the rector of the university, Professor Fevzi Bingöl and Professor Yusuf Calayır of the Department of Civil Engineering for having enabled transportation and logistical support. The METU administration is also acknowledged for the rapid deployment they enabled.

**References**

Akkar S. and Cagnan Z. (2010). A local ground motion predictive model for Turkey and its comparison with other regional and global ground-motion models, submitted to Bull. Seism. Soc. Am. for publication.

N. Ambraseys (2009). Earthquakes in the Mediterranean and Middle East: A Multidisciplinary Study of Seismicity up to 1900, Cambridge University Press.

A. Barka (1996). Slip Distribution along the North Anatolian Fault Associated with the Large Earthquakes of the Period 1939 to 1967, Bull. Seism. Soc. Am. 86, 1238 -1254.

Boore, D. M. Joyner, W. B. and Fumal, T. E. (1997). “Equations for estimating horizontal response spectra and peak acceleration from western North American earthquakes: a summary of recent work”, Seismol. Res. Lett. Vol. 68, pp. 128-153.

Boore, D. M. and Atkinson, G. M. (2008). “Ground motion prediction equations for the average horizontal component of PGA, PGV, and 5%-damped PSA at spectral periods between 0.01 s and 10.0 s”, Earthquake Spectra, Vol. 24, No. 1, pp. 99-138.

Campbell, K. W. and Bozorgnia, Y. (2008). “NGA ground motion model for the geometric mean horizontal component of PGA, PGV, PGD and 5% damped linear elastic response spectra for periods ranging from 0.01 to 10 s”, Earthquake Spectra, Vol. 24, No. 1, pp. 139-172.

Graizer, V. and Kalkan, E. (2007). “Ground motion attenuation model for peak horizontal acceleration from shallow crustal earthquakes”, Earthquake Spectra, Vol. 23, pp. 585–613.

Grünthal, G. (Editor) (1998). European Macroseismic Scale 1998, Cahiers du Centre Européen du Géodymamique et de Séismologie 15, 99.

Kalkan, E. and Gülkan, P. (2004). “Site-Dependent Spectra Derived from Ground Motion Records in Turkey”, Earthquake Spectra, Vol. 20, No. 4, pp. 1111-1138.

Lin, J., and R. S. Stein (2004). Stress triggering in thrust and subduction earthquakes, and stress interaction between the southern San Andreas and nearby thrust and strike-slip faults. Journal of Geophysical Research 109, B02303; doi:10.1029/2003JB002607.

Power, M., Chiou, B., Abrahamson, N. and Roblee C. (2006). “The Next Generation of Ground Motion Attenuation Models” (NGA) project: An overview”, In Proceedings, Eighth National Conference on Earthquake Engineering, Paper No. 2022.

Saroglu, F., Emre, O. and Kuscu, I. (1992). Active fault map of Turkey, MTA, Turkey.

Toda, S., R. S. Stein, K. Richards-Dinger, and S. Bozkurt (2005). Forecasting the evolution of seismicity in southern California: Animations built on earthquake stress transfer. Journal of Geophysical Research B05S16; doi:10.1029/2004JB003415.

Turkish Ministry of Public Works and Settlement (2007). Specification for Structures to be Built in Disaster Areas, TEC-07, Ankara, Turkey.

Utkucu, M., Nalbant, S.S., McCloskey, J., Steacy, S., Alptekin Ö. (2003). Slip distribution and stress changes associated with the 1999 November 12 (Düzce) earthquake (Mw=7.1), Geophys. J. Int., 153, 229-241.

Wells, D., and K. Coppersmith (1994). New empirical relationships among magnitude, rupture length, rupture width, rupture area, and surface displacement, Bull. Seism. Soc. Am. 84, 974 -1002.

Zor E., E. Sandvol, J. Xie, N. Türkelli, B. Mitchell, A. H. Gasanov and G. Yetirmishli (2007). Crustal Structure within the Turkish Plateau and Sorrounding Regions, Bull. Seism. Soc. Am. 97, 151 - 161.

**Table 1.** Selected ground motion records and details of stations (source: http://daphne.deprem.gov.tr).

| Station Information | | | | | | | Distance Measure | | Peak Values (EW), (cm/s²) | | | Peak Values (NS), (cm/s²) | | |
|---|---|---|---|---|---|---|---|---|---|---|---|---|---|---|
| City | Province | Station Code | Latitude | Longitude | Sta. No | $V_{S30}$ (m/s) | $R_{CL}$ (km) | $R_{JB}$ (km) | PGA | SA(0.2s) | SA(1.0s) | PGA | SA(0.2s) | SA(1.0s) |
| Adıyaman | Merkez | 201 | 37.7612 | 38.2674 | 201 | 391 | 192.4 | 191.6 | 2.3 | 2.6 | 2.9 | 2.5 | 2.9 | 4.0 |
| Bingöl | Merkez | 1201 | 38.8971 | 40.5032 | 1201 | 529 | 40.5 | 36.8 | 33.9 | 89.2 | 41.5 | 53.8 | 89.3 | 46.6 |
| Bingöl | Karlıova | 1206 | 39.2935 | 41.0088 | 1206 | 356 | 91.8 | 90.3 | 17.6 | 40.8 | 24.8 | 11.6 | 45.9 | 16.8 |
| Bingöl | Solhan | 1209 | 38.9660 | 41.0499 | 1209 | 463 | 87.0 | 85.4 | 28.9 | 64.3 | 16.8 | 28.9 | 59.4 | 11.2 |
| Diyarbakır | Merkez | 2101 | 37.9309 | 40.2028 | 2101 | 519 | 105.3 | 103.9 | 5.0 | 11.4 | 4.4 | 3.3 | 12.4 | 4.2 |
| Elazığ | Merkez | 2301 | 38.6704 | 39.1927 | 2301 | 407 | 72.4 | 70.1 | 4.5 | 12.1 | 4.4 | 5.5 | 13.2 | 4.7 |
| Elazığ | Palu | 2303 | 38.6958 | 39.9319 | 2303 | 329 | 24.2 | 17.3 | 66.2 | 94.8 | 52.9 | 61.7 | 116.1 | 71.4 |
| Mardin | Merkez | 4701 | 37.3263 | 40.7237 | 4701 | 709 | 182.2 | 181.4 | 2.5 | 2.8 | 1.5 | 2.6 | 2.6 | 1.1 |
| Urfa | Merkez | 6301 | 37.1681 | 38.8014 | 6301 | N/A | 209.0 | 208.3 | 1.4 | 2.6 | 1.3 | 1.6 | 2.9 | 1.9 |
| Batman | Merkez | 7201 | 37.8730 | 41.1511 | 7201 | 450 | 150.3 | 149.3 | 5.4 | 7.6 | 1.3 | 7.6 | 7.5 | 1.0 |
| Erzincan | Merkez | 2401 | 39.7418 | 39.5115 | 2401 | 314 | 104.0 | 102.1 | 6.9 | 18.3 | 17.1 | 8.9 | 30.4 | 10.9 |

**Table 2.** Structural classification of buildings in the affected region

| | |
|---|---|
| Type-I | Non-engineered rural masonry with adobe or stone walls, low quality mortar, heavy earthen roof. EMS vulnerability class A. |
| Type-II | Non-engineered rural masonry with adobe or stone walls in the presence of lintels and horizontal bond beams, low quality mortar, light steel metal roof. EMS vulnerability class B. |
| Type-III | Mixed masonry construction with stone walls in the first story and adobe or hollow factory brick walls in the second story, light steel metal roof. EMS vulnerability class A. |
| Type-IV | Substandard reinforced concrete frame buildings with poor material and construction quality. EMS vulnerability class C. |